

Neural network-assisted personalized handwriting analysis for Parkinson's disease diagnostics

Received: 24 August 2024

Accepted: 8 April 2025

Published online: 02 June 2025

Guorui Chen¹, Trinny Tat¹, Yihao Zhou¹, Zhaoqi Duan¹, Junkai Zhang², Kamryn Scott¹, Xun Zhao¹, Zeyang Liu¹, Wei Wang², Song Li^{1,3}, Katy A. Cross⁴ & Jun Chen¹✉

 Check for updates

Diagnosing Parkinson's disease (PD) promptly, accessibly and effectively is crucial for improving patient outcomes, yet reaching this goal remains a challenge. Here we developed a diagnostic pen featuring a soft magnetoelastic tip and ferrofluid ink, capable of sensitively and quantitatively converting both on-surface and in-air writing motions into high-fidelity, analyzable signals for self-powered PD diagnostics. The diagnostic pen's working mechanism is based on the magnetoelastic effect in its magnetoelastic tip and the dynamic movement of the ferrofluid ink. To validate the clinical potential, a pilot human study was conducted, incorporating both patients with PD and healthy participants. The diagnostic pen accurately recorded handwriting signals, and a one-dimensional convolutional neural network-assisted analysis successfully distinguished patients with PD with an average accuracy of 96.22%. Our development of the diagnostic pen represents a low-cost, widely disseminable and reliable technology with the potential to improve PD diagnostics across large populations and resource-limited areas.

Parkinson's disease (PD) is one of the fastest-growing neurodegenerative diseases, afflicting a substantial 10 million people worldwide^{1–5}. Symptoms of PD, notably, tremors, rigidity and bradykinesia, hinder patient mobility, considerably impacting their quality of life^{6–8}. Conventional procedures to diagnose and monitor PD progression involve the observation of motor symptoms^{9–11}, such as tremors and rigidity. These methods are exceedingly user dependent and inefficient, and are deprived of objective, quantitative standards¹². Moreover, access to subspecialty resources for PD diagnosis is limited, with an insufficient number of neurologists in low-income countries (0.03–0.13 per 100,000 population)¹³. Although recent advances have highlighted the role of biological changes that occur long before the onset of motor symptoms¹⁴, such as the presence or absence of pathological α-synuclein in tissues or body fluids¹⁵, cerebrospinal fluid levels of

L-3,4-dihydroxyphenylalanine decarboxylase¹⁶ and morphological abnormalities in the retina¹⁷ (Supplementary Note 1), the identification of these biomarkers typically requires sophisticated equipment and specialized expertise, which is often available only in centralized healthcare facilities¹⁸. Therefore, a quantitative, low-cost and accessible method for PD diagnosis in large populations remains an unmet clinical need¹⁹.

Handwriting is a complex process that intertwines cognitive, perceptual and fine motor abilities²⁰, all of which are substantially affected by PD²¹. When motor symptoms affect the dominant hand (Supplementary Note 2)^{22–24}, analyzing handwriting patterns could offer crucial insights and quantitative biometric markers for diagnosing the disease²⁵. Although conventional handwriting analysis tools such as digital tablets or screens are widely utilized²⁶, they typically

¹Department of Bioengineering, University of California, Los Angeles, Los Angeles, CA, USA. ²Department of Computer Science, University of California, Los Angeles, Los Angeles, CA, USA. ³Department of Medicine, University of California, Los Angeles, Los Angeles, CA, USA. ⁴Department of Neurology, University of California, Los Angeles, Los Angeles, CA, USA. ✉e-mail: jun.chen@ucla.edu

specialize in tracking handwriting trajectories and analyzing the resulting handwriting traces, often overlooking the motor symptoms that manifest during writing. In addition, their cost and complex setup may pose challenges for broader implementation and limit their practicality for continuous monitoring in everyday, nonclinical settings.

Here, we developed a diagnostic pen featuring a magnetoelastic tip and ferrofluid ink designed to sensitively convert subtle on-surface and in-air writing motions into high-fidelity sensing signals for self-powered handwriting analysis. Pressure applied during handwriting induces deformation of the magnetoelastic tip, leading to a shift in the magnetic flux through the magnetoelastic effect. This flux variation, combined with the dynamic movement of the ferrofluid ink during handwriting, generates voltage signals in the surrounding coil. Beyond its functionality, the diagnostic pen is cost-effective, is scalable in fabrication and demonstrates long-term stability and reliability under various usage conditions. To demonstrate its clinical potential, we conducted a pilot human study involving 3 patients with PD and 13 healthy participants. The diagnostic pen accurately recorded handwriting signals. Neural network-assisted analysis of these handwriting signals successfully distinguished patients with PD from healthy participants with an average accuracy of 96.22%. In summary, our study demonstrates that the self-powered diagnostic pen provides a potential low-cost, widely disseminable, reliable and accessible strategy for the timely detection of PD. This diagnostic pen technology could offer an innovative pathway to complement existing PD diagnostic methods by supporting a crowd-sourced approach, facilitating early detection in large populations. It is particularly beneficial for untreated individuals who may not yet recognize themselves as potential patients with PD and for those in resource-limited regions where access to medical diagnostics using chemical biomarkers is scarce.

Results

Design and working mechanism

Our diagnostic pen (Fig. 1a) consists of two main components: a magnetoelastic tip and ferrofluid ink. The magnetoelastic tip is securely connected to the top of the three-dimensionally (3D) printed barrel, allowing stable integration of the components. The ferrofluid ink is housed in a replaceable plastic reservoir equipped with a cap designed to prevent leakage and evaporation. All components are integrated into the barrel. Conductive yarn is woven into a coil structure that converts variations in magnetic flux into high-fidelity voltage signals for handwriting analysis. Finally, the coil is enclosed in a polyolefin grip, providing a slip-resistant surface.

The magnetoelastic tip is fabricated by embedding the magnetic particles in a silicone matrix and subsequently magnetizing the assembly (Fig. 1b and Supplementary Fig. 1). The magnetoelastic tip brings two functionalities to the diagnostic pen: (1) it generates a vertical magnetic field to sustain magnetization within the ferrofluid ink (Fig. 1c), and (2) under external mechanical stress (Fig. 1d), the tip deforms (Fig. 1e), altering the orientation and spacing of its embedded magnetic particles, which results in a shift in its magnetic flux. This flux variation, combined with the dynamic movement of the ferrofluid ink within the diagnostic pen, leads to changes in the net magnetic flux through the surrounding coil, thereby inducing a voltage according to Faraday's law of induction. The ferrofluid ink consists of single-domain nanomagnets (Fig. 1f) exhibiting superparamagnetic behavior (Extended Data Fig. 1a,b)^{27–29}. The nanomagnets are coated with an oleic acid surfactant and dispersed in the carrier solution, with a mean particle diameter of 7.13 ± 1.40 nm (Extended Data Fig. 1c,d). The superparamagnetic behavior exhibited by the nanomagnets allows the ferrofluid ink to respond rapidly to fluctuations in the external magnetic field (Extended Data Fig. 1e–g).

To deepen our understanding of the magnetoelastic tip–ferrofluid ink chemical system (Supplementary Fig. 2), we initiated an investigation into the fluid dynamics and magnetic interactions (Fig. 1g). When

the external magnetic field is positioned far from the ferrofluid ink, inducing only weak magnetization, the ferrofluid ink flows freely (Fig. 1g, left). When an external magnetic field is applied near the ferrofluid ink, inducing strong magnetization (Fig. 1g, right), the ink forms a spiky pattern on its surface due to the normal field (Rosensweig) instability (Supplementary Video 1)^{30–32}. This instability occurs because the electromagnetic (Maxwell) stress pulls the fluid into peaks, while surface tension and gravity act to flatten the surface, creating a balance that results in the characteristic spiked pattern (Extended Data Fig. 1h–j and Supplementary Note 3). The rapid response to changes in the external magnetic field (Supplementary Video 2) can be attributed to the ferrofluid ink's low coercivity and saturation remanence (Supplementary Fig. 3).

Meanwhile, the magnetoelastic tip demonstrated a high remanence value³³, enabling it to emerge as a stable and permanent magnetic field source. After impulse magnetization, the magnetoelastic tip provided a magnetic field accompanied by a surface magnetic flux capable of reaching 70 mT (Supplementary Fig. 4). This vertically distributed magnetic field magnetizes the ferrofluid ink (Fig. 1h and Supplementary Note 4). Moreover, after the ferrofluid ink in the diagnostic pen is periodically used over an extended period, both the viscosity of the ferrofluid ink and the magnetic properties of the magnetoelastic tip–ferrofluid ink system remain stable, showing no noticeable variation (Fig. 1i). These results support the pen's stability for practical applications.

Finally, we quantified the magnetoelastic effect in the magnetoelastic tip by measuring its magnetomechanical coupling factor (d_{33}), defined as the magnetic flux variation under applied stress. We determined d_{33} from the slope of the curves in Fig. 1j after converting force into the stress units. Within the range of forces applied during handwriting, the magnetoelastic tip deforms and exhibits a d_{33} of up to 4.9×10^{-8} T Pa⁻¹ in the vertical direction. These results confirm that the magnetoelastic tip can effectively convert handwriting pressure into magnetic flux variations, inducing voltage signals in the vertically positioned coil above. In summary, the diagnostic pen's working mechanism—driven by the magnetoelastic effect in the soft tip and the dynamic movement of the ferrofluid ink—enables the conversion of handwriting motor symptoms into sensing signals.

Scalable fabrication and characterization

Scalable fabrication and wide disseminability of the diagnostic pen are essential for its potential adoption in clinical settings. The diagnostic pen's design, featuring a barrel structure, enables efficient and scalable production via 3D printing. This straightforward design results in a total weight (Supplementary Table 1) comparable to commercial electronic pens, ensuring comfort during prolonged use. Meanwhile, the ferrofluid ink can be loaded into a replaceable ink reservoir using an automated handler (Fig. 2a), making the process compatible with industrial-scale manufacturing. The reservoir is securely sealed with a robust cap to prevent leaks and evaporation, ensuring stability and reliability for long-term use. This scalable manufacturing process, combined with the low cost of raw materials (Supplementary Table 2), makes the magnetoelastic diagnostic pen a practical and cost-effective solution.

For the as-fabricated diagnostic pen, the magnetoelastic tip generates a vertical magnetic field to sustain magnetization within the ferrofluid ink (Fig. 2b). The integration of the magnetoelastic tip and ferrofluid ink, as shown in the schematic (Fig. 2c) and cross-sectional view (Fig. 2d), enables the diagnostic pen to function via the magnetoelastic effect and ferrofluid dynamics, allowing it to track multiple motion patterns during handwriting. Hand movements during handwriting can be categorized into two types: in-air movements, where the pen moves between strokes without surface contact, and on-surface movements, where the pen contacts the writing surface and experiences pressure, forming primary strokes. During in-air movements, the operating principle involves acceleration measurements from

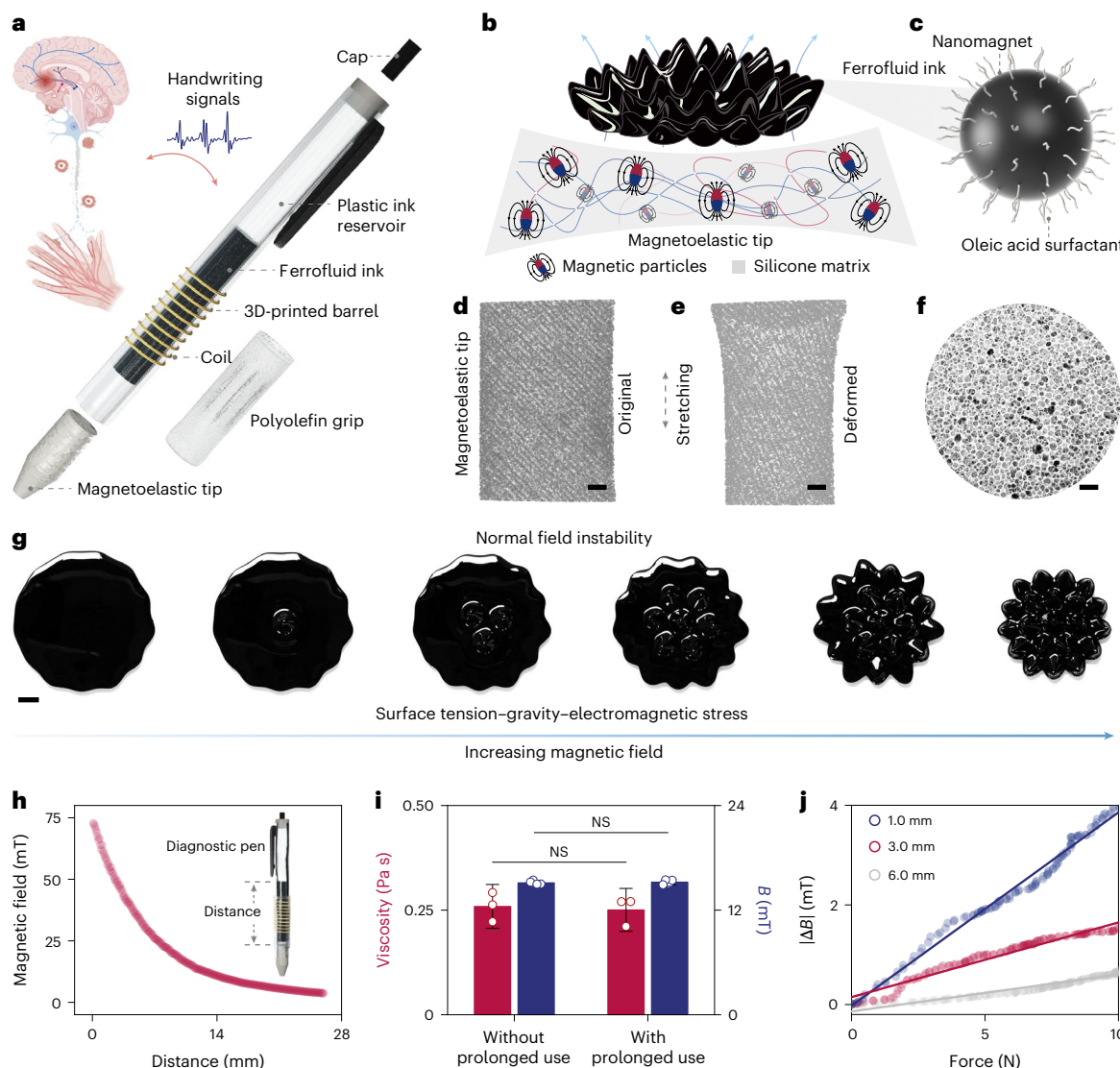


Fig. 1 | Design and working mechanism of the magnetoelastic diagnostic pen. **a**, An illustration of the diagnostic pen for personalized handwriting analysis and PD diagnostics. **b**, The diagnostic pen comprises a magnetoelastic tip and ferrofluid ink, with the tip consisting of magnetic particles embedded in a silicone matrix. **c**, The ferrofluid ink is composed of single-domain nanomagnets. **d,e**, Micro-CT images of the magnetoelastic tip materials in two distinct states: the original state (before stretching) (**d**) and the deformed state (after stretching) (**e**). Scale bars, 1.5 mm. **f**, A transmission electron microscopy image of magnetic nanoparticles. Scale bar, 25 nm. **g**, The surface topography of the ferrofluid ink under different external magnetic fields, governed by the balance of surface

tension, gravity and electromagnetic stress. Scale bar, 3 mm. **h**, The magnetic field distribution of the magnetoelastic tip along the vertical direction. **i**, The viscosity (red) of the ferrofluid ink and the magnetic properties (blue) of the magnetoelastic tip–ferrofluid ink system show no noticeable variation between samples with and without prolonged use. Data are presented as mean \pm s.d.; $n = 3$ experiments (viscosity) and 5 testing points (magnetic flux). Significance was determined by a two-tailed *t*-test. NS, not significant. **j**, The absolute value of magnetic flux variation at various vertical distances from the magnetoelastic tip under applied force. Panel **a** created with BioRender.com.

the movement of the magnetized ferrofluid ink (Fig. 2e and Supplementary Note 5)^{34–36}. During on-surface movements, in addition to the ferrofluid ink's dynamic movement, the diagnostic pen also leverages the deformation of its soft magnetoelastic tip. The dynamic pressure applied to the magnetoelastic tip causes it to deform, which shifts the magnetic flux due to the magnetoelastic effect (Fig. 2f). This variation in magnetic flux, combined with the movement of the ferrofluid ink, generates voltage signals in the coil. Strain–stress testing results confirmed that handwriting pressure can deform the soft magnetoelastic tip (Fig. 2g). Moreover, as prolonged handwriting may raise the diagnostic pen's temperature close to body temperature, we investigated the stability of the ferrofluid ink under temperature fluctuations. The results (Fig. 2h) show that the viscosity–shear rate curves measured at room temperature (25 °C) and typical hand temperature (33 °C)

exhibit no notable variation. Similarly, magnetic flux measurements of the magnetoelastic tip–ferrofluid ink system showed consistent values between the two temperatures (Fig. 2i). These findings confirm the stability of the ferrofluid ink across the tested temperature range, ensuring reliable performance during prolonged handwriting analysis (Supplementary Note 6).

To further demonstrate the ferrofluid ink's ability to detect subtle, high-frequency motions during handwriting, we conducted a series of tests. We pumped air through the magnetized ferrofluid ink (Fig. 2j) to simulate the subtle mechanical excitations that occur during the operation of the diagnostic pen. A copper-wired coil was positioned underneath the ink and successfully collected the high-fidelity voltage signals (Fig. 2k). In addition, we released droplets onto the magnetized ferrofluid ink to apply a gentle mechanical force. This event

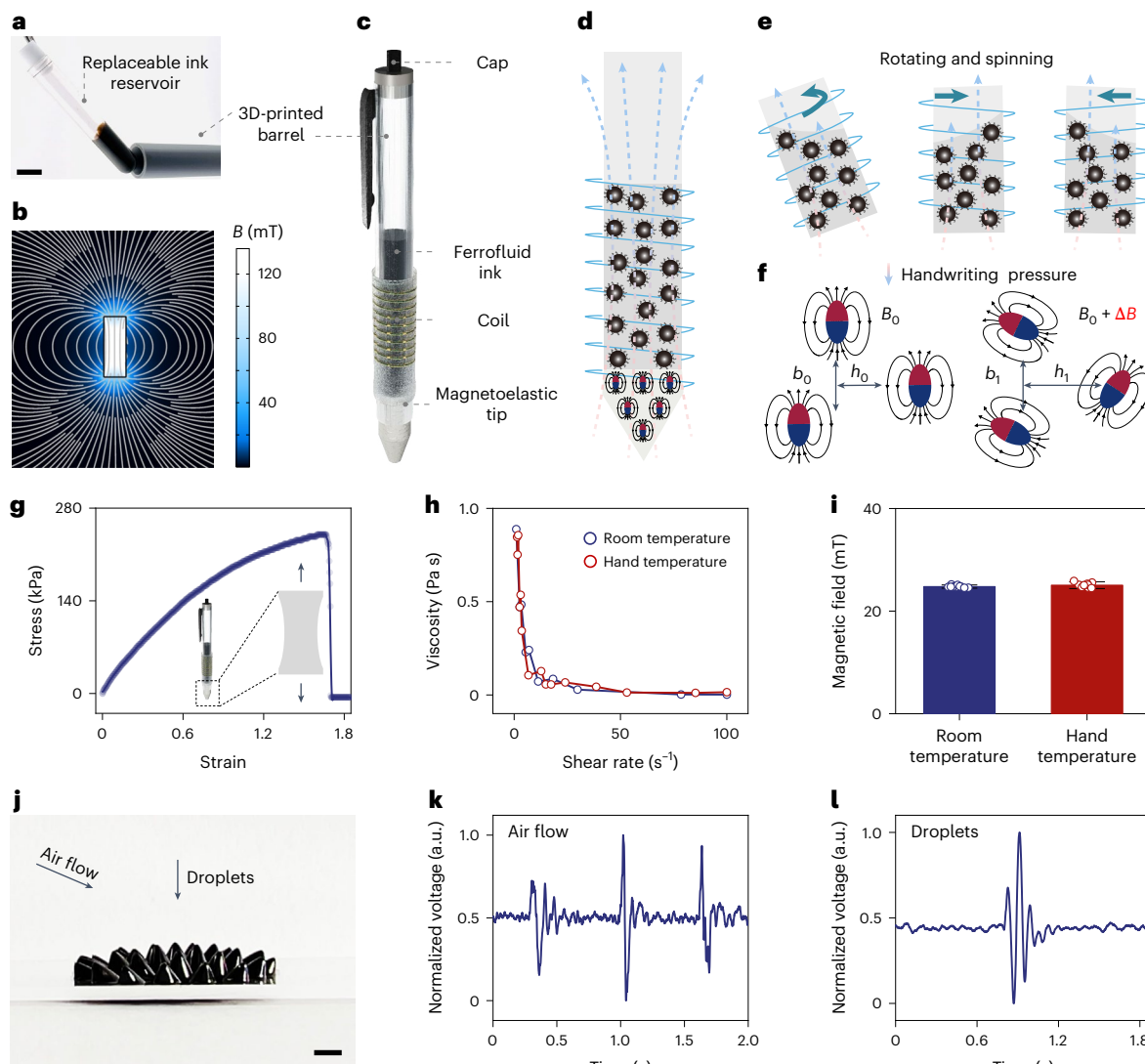


Fig. 2 | Fabrication and characterization. **a**, The ferrofluid ink is securely stored in a replaceable ink reservoir sealed with a cap. Scale bar, 1 cm. **b**, Simulation results of the spatial magnetic field distribution. **c**, A schematic illustration of the magnetoelastic tip–ferrofluid ink system in the diagnostic pen. **d**, A schematic illustration of the cross-sectional view of the magnetoelastic tip–ferrofluid ink system in the diagnostic pen. **e,f**, The diagnostic pen operates through the dynamic movement of the ferrofluid ink (**e**) and the magnetoelastic effect in the magnetoelastic tip (**f**), both of which contribute to magnetic field variations and thereby induce voltage signals. **b**, vertical distances; **h**, horizontal distances;

g, Stress–strain testing of the magnetoelastic tip. **h**, Viscosity–shear rate curves of the ferrofluid ink at room temperature and hand temperature. **i**, Magnetic properties of the magnetoelastic tip–ferrofluid ink system at room temperature and hand temperature. Data are presented as mean \pm s.d.; $n = 10$ testing points. **j**, A photograph of the magnetized ferrofluid ink for voltage signal generation. Scale bar, 3 mm. **k**, Voltage generation associated with continuous air flow over time. **l**, Voltage generation over time with droplet release.

generated voltage signals, which we attributed to the gravitational pressure exerted by the falling droplet (Fig. 2*l*). These results highlight the system's high sensitivity and accuracy in converting subtle mechanical motions into real-time voltage signals.

Handwriting-to-electrical signal conversion

To assess the handwriting-to-electrical signal conversion process, we simulated the mechanical movements of handwriting (Supplementary Fig. 5), segmenting the complex gestures into horizontal (Supplementary Fig. 6) and vertical (Supplementary Fig. 7) motions. We first investigated the current signals induced by motions in varying horizontal accelerations (Fig. 3*a*), horizontal frequencies (Fig. 3*b*), vertical accelerations (Fig. 3*c*) and vertical frequencies (Fig. 3*d*). The procedure revealed a clear increase in the current signal output with rising acceleration levels, as shown in Fig. 3*a* (horizontal) and Fig. 3*c* (vertical). This observation aligns with the principle

that higher acceleration causes the ferrofluid ink to move more rapidly, resulting in magnetic flux variations occurring over a shorter time interval. In addition, the effect of sinusoidal waveforms with varying frequencies on the current signal output is shown in Fig. 3*b* (horizontal) and Fig. 3*d* (vertical). The results show that higher-frequency movements generate stronger output signals, which can be attributed to the diagnostic pen's working mechanism. According to Faraday's law of induction, the induced electromotive force is proportional to the rate of change of magnetic flux. Under high-frequency mechanical excitation, the magnetic field of the diagnostic pen fluctuates more rapidly, resulting in amplified current signals.

During handwriting, various motions occur, resulting in a complex combination of vertical (Supplementary Fig. 8) and horizontal movements (Supplementary Fig. 9) of the diagnostic pen. In addition to capturing time-domain information, such as acceleration and handwriting frequency, the diagnostic pen can also collect the pressure variations,

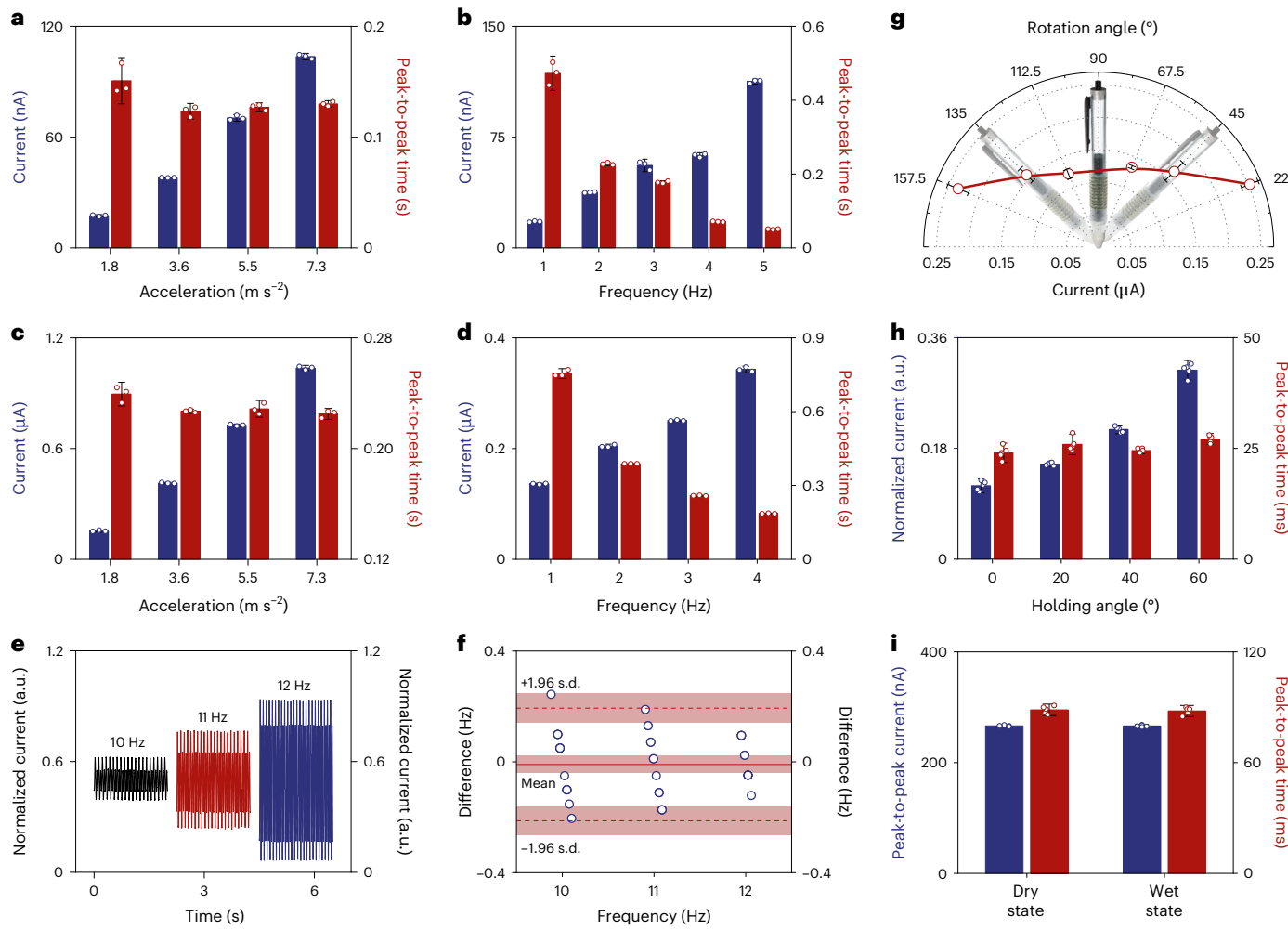


Fig. 3 | Converting handwriting into high-fidelity sensing signals.

a,b, Correlation of the magnetoelastic diagnostic pen's current outputs (blue) and the peak-to-peak time interval (red) with different acceleration levels (**a**) and frequencies (**b**) under horizontal movements. Data are presented as mean \pm s.d.; $n = 3$ movement cycles. **c,d**, Correlation of the diagnostic pen's current outputs (blue) and the peak-to-peak time interval (red) with different acceleration levels (**c**) and frequencies (**d**) under vertical movements. Data are presented as mean \pm s.d.; $n = 3$ movement cycles. **e**, Time-varying current output analysis of diagnostic pen under high-frequency movements. **f**, A Bland–Altman plot

illustrating the calculated frequency aligning with the ground truth, validating measurement accuracy. **g**, Current output analysis of the diagnostic pen with different rotation angles of $\pm 22.5^\circ$, $\pm 45^\circ$ and $\pm 67.5^\circ$. **h**, Correlation of the diagnostic pen's current outputs (blue) and the peak-to-peak time interval (red) with different holding angles. Data are presented as mean \pm s.d.; $n = 5$ movement cycles. **i**, The diagnostic pen's current outputs (blue) and the peak-to-peak time interval (red) under the dry and wet states. Data are presented as mean \pm s.d.; $n = 5$ movement cycles.

which are critical for detecting handwriting abnormalities. Our results show that, during on-surface vertical movements, the current signals exhibited a linear correlation with handwriting pressure within the range of 20–110 kPa, with an R^2 value of 0.98 (Supplementary Fig. 10). This capability to capture both time-domain information and handwriting pressure enables the diagnostic pen to track a broader range of motor symptoms that manifest during handwriting, providing a foundation for detecting abnormalities in hand movements.

We investigated the diagnostic pen's ability to capture high-frequency handwriting movements. The results demonstrated that the diagnostic pen accurately recorded high-frequency movements in the range of 10–12 Hz (Fig. 3e). In addition, a Bland–Altman plot (Fig. 3f) indicated that the frequencies calculated from the diagnostic pen's signals closely align with the ground truth, confirming its measurement accuracy. As human handwriting typically occurs at frequencies below 5 Hz, these findings validate the diagnostic pen's capability to precisely record fast handwriting movements without noticeable lag, confirming its suitability for high-frequency motion detection.

Furthermore, during handwriting, the pen is often rotated to adjust the angle. We examined the impact of rotating the diagnostic pen at

different angles, including $\pm 22.5^\circ$, $\pm 45^\circ$ and $\pm 67.5^\circ$ (Fig. 3g). This showed that output currents were amplified when subject to larger angles of rotation, regardless of the direction of the diagnostic pen's rotation. We also investigated the impact of different holding angles on the diagnostic pen's sensing performance, testing angles from 0° (vertical) to 60° . The results showed that the peak-to-peak time exhibited no substantial variation across all tested angles (Fig. 3h, red), indicating that time-domain information remains stable despite changes in holding angle. This aligns with the diagnostic pen's working principle, where time-domain characteristics depend solely on the input handwriting movements. Meanwhile, the signal amplitude increased with larger holding angles (Fig. 3h, blue). This occurs because, at steeper angles, gravity shifts the ferrofluid ink away from the magnetoelastic tip, increasing its dynamic movement. Further analysis revealed a strong linear relationship ($R^2 = 0.94$) between the holding angle and signal amplitude (Supplementary Fig. 11). Thus, the impact of different holding angles on the sensing signal amplitudes could be calibrated through a personalized calibration procedure.

Finally, we evaluated the stability of the diagnostic pen in practical handwriting applications. After 10,000 cycles of continuous

mechanical excitation (Supplementary Fig. 12), the diagnostic pen's current signals remained stable, indicating no substantial variation in signal output and demonstrating its prolonged durability. Moreover, the diagnostic pen provides waterproof properties, ensuring stable performance despite hand perspiration. As shown in Fig. 3*i*, the diagnostic pen maintained stable functionality without performance degradation, even after being sprayed with water while wet. In addition, we tested the diagnostic pen's reliability across diverse writing environments (Supplementary Note 7). The results indicate that differences in the tested writing surfaces have limited impact on signal generation. These findings demonstrate the diagnostic pen's robust sensing performance and resilience against environmental variations.

Personalized handwriting analysis

Building on the diagnostic pen's demonstrated capability to convert handwriting biomechanical signals into high-fidelity sensing signals, we now explore its potential in clinical scenarios, specifically through a pilot human study aimed at personalized handwriting analysis for PD diagnostics (Fig. 4*a*). Handwriting, one of the most common daily activities, is derived from the complex interaction between personal cognitive, kinesthetic and perceptual-motor abilities (Fig. 4*b*). While this intricate process is taken for granted by many, it becomes exceedingly difficult for those afflicted by PD³⁷. PD is a progressive and chronic neurodegenerative disorder attributed to the gradual loss of dopamine-producing neurons in the brain³⁸, adversely affecting fine motor skills, including those utilized while writing³⁹. Compared with healthy participants, patients with PD often exhibit manifestations of tremors and bradykinesia in the hands and fingers, which can alter handwriting patterns long before a formal diagnosis is made⁴⁰. These abnormalities could be tracked by using the developed diagnostic pen. For instance, simulated hand tremors are recorded as additional minor peaks (Fig. 4*c*, highlighted by the box), distinguishing them from the patterns of normal handwriting.

To validate our technology for personalized handwriting analysis, a pilot human study was executed at the Ronald Reagan University of California, Los Angeles (UCLA) Medical Center (approved IRB no. 21-0000974) (Extended Data Fig. 2 and Supplementary Note 8). The participant cohort, consisting of both healthy participants and patients with PD (Supplementary Note 9), was recruited for the pilot study. After providing informed consent (Supplementary Note 10), participants were instructed to use the diagnostic pen to complete a series of tasks (Extended Data Fig. 3a and Supplementary Note 11)²⁶. These tasks included task 1 (illustrating continuous wavy lines; Supplementary Fig. 13a), task 2 (illustrating continuous spirals; Supplementary Fig. 13b) and task 3 (writing six capital letters 'MEGPEN'; Supplementary Fig. 13c). These tasks were performed both on the surface (Extended Data Fig. 3b-d) and in the air (Extended Data Fig. 4).

For healthy participants, representative current signals from three different individuals (participants 1–3) during handwriting, collected using the diagnostic pen, are shown in Fig. 4*d* (writing on the surface) and Fig. 4*e* (writing in the air). The top, middle and bottom rows of Fig. 4*d,e* are representative of the current signals induced by task 1 (illustrating continuous wavy lines; Supplementary Fig. 14), task 2 (illustrating continuous spirals; Supplementary Fig. 15) and task 3 (writing 'MEGPEN'; Supplementary Fig. 16), respectively. The left, middle and right columns of Fig. 4*d,e* incorporate the current signals executed by participant 1, participant 2 and participant 3, respectively. Based on the accumulated sensing signals, we concluded the following. (1) The on-surface writing movements (blue) and the in-air writing movements (red) were both recorded with high fidelity. In particular, the on-surface writing movements invoked increased current values, which was attributed to the combination of magnetoelastic tip deformation and the movement of the ferrofluid ink. (2) In comparison with task 1 and task 2, task 3 has amplified peak current values, as writing specific letters (task 3) involves more dynamic interactions between the magnetoelastic tip and the paper than merely illustrating a continuous line (task 1 and task

2). These magnetoelastic tip actions induce dynamic shifts in pen-to-paper pressure, thereby rapidly generating magnetic field variations and inducing elevated peak current values. (3) In addition, we found that quantitative handwriting parameters, such as peak-to-peak current values and cycle duration of these tasks, can be extracted from the writing signals (Fig. 4*f*). The variations observed in these parameters can be explained by factors such as differences in writing experience and individual variations in motor execution.

The recruited patients with PD were instructed to perform the writing tasks (Supplementary Fig. 17), both on the surface and in the air (Supplementary Video 3). The experimental results demonstrated that both the on-surface and in-air writing movements could be recorded with high fidelity (Supplementary Fig. 18). Specifically, as shown in Fig. 4*g*, each cycle of task 1 was accurately recorded, with the five major peaks corresponding to the writing strokes used to draw five continuous wavy lines. In addition, these representative handwriting signals of a patient with PD exhibited minor peaks during writing (Fig. 4*g*, dotted box). To further conduct personalized handwriting analysis of patients with PD and healthy participants, we selected writing cycles from the same task performed by the same individuals, and handwriting parameters were extracted, including the peak current values normalized to their mean and the writing duration for each cycle (Fig. 4*h*). Based on the acquired data, the signals of the patient with PD exhibited peak current values of 1.33 ± 0.40 arbitrary units (a.u.) with a writing duration of 4.28 ± 0.35 s, whereas the healthy participant's signals showed peak current values of 0.67 ± 0.11 a.u. with a writing duration of 2.97 ± 0.27 s. These observations, although based on a limited dataset from our pilot human study, provide support for the diagnostic pen's potential to accurately capture handwriting movements in clinically relevant application scenarios.

Neural network-assisted PD diagnostics

Finally, we implemented a neural-network-assisted analysis to differentiate the handwriting signals of patients with PD from those of healthy individuals (Fig. 4*i* and Supplementary Note 12). We evaluated three neural-network-based models, including a one-dimensional convolutional neural network (1D CNN), 1D CNN with long short-term memory (LSTM) and LSTM, alongside three traditional machine learning methods (random forest, XGBoost and logistic regression). These models were used to classify handwriting signals from a cohort of 16 individuals, including 3 patients with PD. All collected handwriting signals underwent standardization by subtracting the mean and dividing by the standard deviation (s.d.). In addition, the signals were segmented into uniform slices. To ensure an unbiased evaluation and prevent test data contamination, we allocated data from different individuals into training and testing sets. Specifically, we reserved the data from one patient with PD and three healthy participants as 'unseen' for testing, while the remaining data were used for training and validation. To ensure robustness, the experiment was repeated over ten random seeds. Comprehensive performance metrics, including accuracy, precision, recall and F1 score, were compared across all models (Fig. 4*j* and Table 1).

Our results show that the 1D CNN model provided an optimal accuracy (0.9622 ± 0.0251) and F1 score (0.9266 ± 0.0523), indicating its ability to extract local patterns from handwriting signals. Its metrics show that healthy participant recall is 0.9795 ± 0.0133 with a precision of 0.9701 ± 0.0297 , while PD recall is 0.9150 ± 0.0873 with a precision of 0.9432 ± 0.0360 , meaning it rarely misses either class (few false negatives) and seldom confuses one class for the other (few false positives) (Fig. 4*k*). These results demonstrate that our diagnostic pen, combined with a neural network-driven handwriting analysis pipeline, holds potential for effective PD diagnosis. Meanwhile, our comparative analysis of different machine learning methods (Table 1) highlights the importance of capturing short-range correlations over long-distance dependencies in handwriting signals for PD diagnosis. This finding aligns with clinical observations and our experimental results, wherein handwriting signals from patients with PD could exhibit localized patterns, such

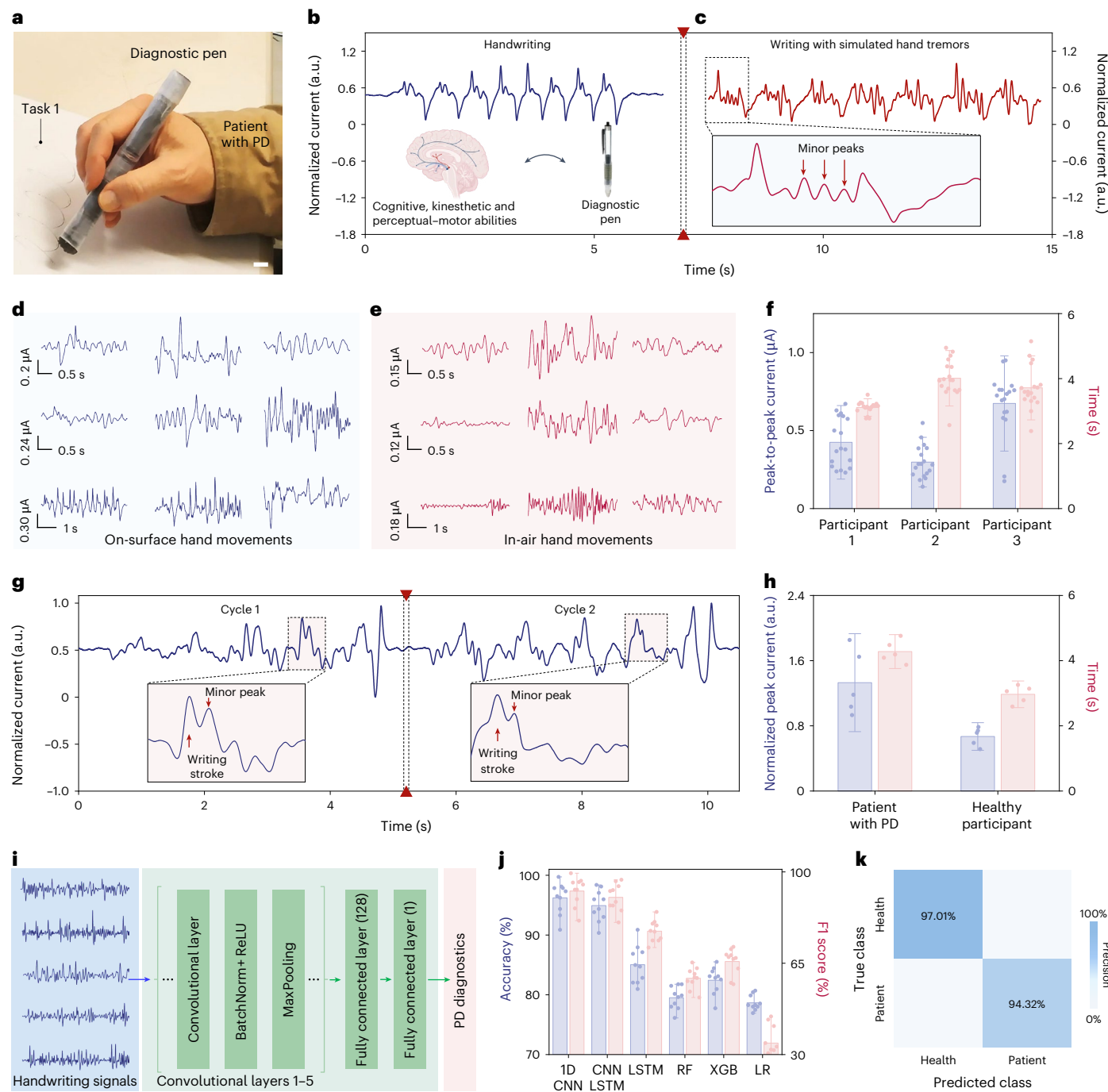


Fig. 4 | Neural network-assisted personalized handwriting analysis for PD diagnostics with pilot human studies. **a**, A patient with PD uses the diagnostic pen to perform task 1 (illustrating continuous wavy lines) in pilot human studies. Scale bar, 1 cm. **b**, The recorded normal handwriting signals result from a complex interplay of cognitive, kinesthetic and perceptual-motor functions. **c**, Handwriting signals with simulated hand tremors. The tremor-affected signals display additional minor peaks (highlighted in the box). **d,e**, Representative current signals from the recruited healthy participants during three handwriting tasks on-surface (**d**) and in air (**e**). The top, middle and bottom rows represent the current signals induced by task 1 (illustrating continuous wavy lines), task 2 (illustrating continuous spirals) and task 3 (writing 'MEGPEN'), respectively. The left, middle and right columns represent the current signals performed by participant 1, participant 2 and participant 3, respectively. **f**, Comparative peak to

peak current values and writing times of different participants. Data are presented as mean \pm s.d.; $n = 18$ movement cycles (blue) and 18 handwriting task cycles (red). **g**, Two cycles of current signals from the handwriting task of a patient with PD. **h**, Normalized peak current values and writing duration extracted from handwriting signals of the same task performed by the same individuals. Data are presented as mean \pm s.d.; $n = 5$ movement cycles (blue) and 5 handwriting task cycles (red). **i**, Personalized handwriting analysis for PD diagnosis using a 1D CNN model. **j**, Comparison of testing accuracy and F1 score across different machine learning models, including 1D CNN, 1D CNN + LSTM, LSTM, random forest (RF), XGBoost (XGB) and logistic regression (LR). Data are presented as mean \pm s.d.; $n = 10$ random seeds. **k**, Class-wise precision in the classification results of the testing dataset using the 1D CNN model. Panel **b** created with BioRender.com.

as minor peaks, which are essential for accurate disease detection. It is important to note that these results are based on our handwriting dataset obtained through this pilot human study. With the increasing

availability of handwriting data collected using our diagnostic pen in future clinical trials, more complex architectures—such as transformer-based models^{41–43}—may become preferable.

Table 1 | Performance evaluation of different machine learning models

	Accuracy	F1 score	Precision (HP and PD)	Recall (HP and PD)
1D CNN	0.9622±0.0251	0.9266±0.0523	0.9701±0.0297 0.9432±0.0360	0.9795±0.0133 0.9150±0.0873
1D CNN + LSTM	0.9493±0.0250	0.9023±0.0506	0.9614±0.0330 0.9270±0.0645	0.9714±0.0289 0.8890±0.0975
LSTM	0.8504±0.0300	0.7728±0.0391	0.9746±0.0115 0.6565±0.0515	0.8168±0.0371 0.9420±0.0260
Random forest	0.7952±0.0180	0.5923±0.0381	0.8446±0.0142 0.6359±0.0426	0.8828±0.0184 0.5560±0.0474
XGBoost	0.8244±0.0215	0.6566±0.0471	0.8687±0.0186 0.6910±0.0471	0.8960±0.0225 0.6290±0.0630
Logistic regression	0.7866±0.0119	0.3440±0.0615	0.7755±0.0102 0.9690±0.0219	0.9974±0.0017 0.2110±0.0466

Evaluation metrics for the classification results on the testing set, including accuracy, precision, recall and F1 score. HP, healthy participants; PD, patients with PD. Results from ten random seeds.

In addition, training a deep learning model from the ground up might require considerable computational resources and extensive data, especially considering the future application of the diagnostic pen in large populations. We demonstrated that leveraging robust, pretrained models^{44,45} through transfer learning offers a potential solution to reduce new data requirements while maintaining high predictive accuracy in detecting patients with PD (Supplementary Note 13)⁴⁶. This approach could minimize participant fatigue and enhance the scalability of our diagnostic pipeline. In brief, the pilot human study demonstrates that the diagnostic pen can accurately convert handwriting into sensing signals. Neural network-assisted analysis of these signals further demonstrates the diagnostic pen's ability to distinguish patients with PD from healthy participants.

Discussion

The diagnostic pen features a chemical system that integrates soft magnetoelastic materials with ferrofluid ink, enabling high-fidelity signal capture from both on-surface and in-air handwriting without the need for external power sources. Demonstrated through pilot human studies, the pen shows potential as a low-cost, accessible tool for PD diagnosis, with potential scalability for broader population use and the prospect of addressing critical gaps in clinical care (Supplementary Note 14). Meanwhile, our diagnostic pen distinguishes itself from traditional micrographic measurement by focusing on motor symptoms exhibited during the act of writing⁴⁷, delivering insights directly tied to PD motor symptoms. By concentrating on motor actions rather than the resultant handwriting outcomes, our technology avoids any potential biases of chirography analysis, offering a potentially more symptom-oriented evaluation. In addition, compared with traditional video technology for PD assessment, our diagnostic pen offers a cost-effective, user-friendly, privacy-conscious and widely accessible solution (Supplementary Note 15). The diagnostic pen is more affordable than video recording equipment and is designed for intuitive use, requiring no specialized skills. Built on the familiarity of handwriting, it is highly user-friendly, accessible and easily disseminable for end users. Operating without external power, the diagnostic pen maintains reliability across various environments commonly encountered in home settings. In addition, it enhances privacy by avoiding the collection of identifiable data. These advantages make the diagnostic pen a practical, accessible and scalable solution for PD diagnostics, with potential scalability in large populations. This diagnostic technology could be especially valuable for individuals who remain undiagnosed due to unrecognized symptoms, as well as those in regions with restricted access to medical resources for chemical biomarker-based diagnosis.

It is worth noting that our findings are based on a pilot human study with a limited sample size. Future studies could involve a more diverse cohort of patients with PD with a large sample size to further

validate the diagnostic-pen-generated handwriting signals as a digital biomarker^{48–52}, along with validation against appropriate clinical criteria to ensure clinical relevance. In our current study, we classified the 3 patients with PD from a group of 13 healthy participants by analyzing handwriting signals recorded by the diagnostic pen. However, it is important to recognize that the feasible biomarker for classification might not be directly applicable to longitudinal assessment or evaluation of disease severity across different stages of PD^{53,54}. Future work could involve patients with PD with known and varying disease stages to further investigate the diagnostic pen's potential for stage evaluation and for tracking disease progression over time⁵⁵. Moreover, our current study is based on cases where motor symptoms affect the dominant hand, as PD typically presents with asymmetrical motor impairment. Although previous clinical studies have shown that the dominant side is affected first in the majority of both left- and right-handed patients with PD^{22–24}, future investigations could also examine the relatively smaller subgroup in which motor symptoms primarily impact the nondominant hand. Such studies may help to clarify the corresponding variations in handwriting signals captured by our diagnostic pen in these cases.

The sensing performance of the diagnostic pen depends on the chemical stability and mechanical properties of the ferrofluid ink and soft magnetoelastic tip. Future work that focuses on tuning these properties by manipulating magnetic particle interactions could guide the development of diagnostic pens with customized stability, motion sensitivity and frequency detection ranges. In addition, as the diagnostic pen potentially transitions into practical, everyday use, the anticipated increase in collected handwriting data may require expanded data storage capacity. Integrating data storage modules directly with the diagnostic pen could facilitate improved data collection and recording processes⁵⁶. Furthermore, implementing wireless synchronization capabilities to transfer data seamlessly into personalized cloud-based datasets could enhance usability and efficiency⁵⁷. Currently, our approach relies on nearby terminals, such as laptops, to run machine learning models for handwriting analysis. Future studies could explore the integration of in-sensor computing modules within the diagnostic pen itself^{58,59}, further enhancing the accessibility of this diagnostic technology, particularly in resource-limited settings. Finally, with the anticipated growth in the availability of handwriting data collected by the diagnostic pen, systematic regulation and management of data privacy will become essential⁶⁰. Establishing robust privacy safeguards will encourage end users to share anonymized handwriting data for large-scale research initiatives or crowd-sourced health projects, ultimately benefiting the management and understanding of PD. Given its broad scientific and societal impacts, we anticipate that this diagnostic pen technology could be of potential relevance for academic, industrial and clinical communities, while also promoting the exchange of ideas across neighboring disciplines such as physics, chemistry, materials science, bioengineering and neuroscience.

Methods

Fabrication of the diagnostic pen

Ecoflex 00-30 part A (Smooth-on) and Ecoflex 00-30 part B (Smooth-on) with a weight ratio of 1:1 were blended and precured at room temperature. Then, neodymium–iron–boron magnets were integrated with the polymer mixture, after which the stirred mixture was poured into the template and cured at 70 °C in an oven (Thermo Fisher Scientific) for 4 h. By utilizing different templates, magnetoelastic soft materials with the given tip structure could therefore be fabricated. The cured magnetoelastic tip was magnetized by an impulse field (approximately 2.65 T) using an impulse magnetizer (IM-10-30, ASC Scientific) to establish the remnant magnetization. The barrel of the diagnostic pen was fabricated using an F123 Composite-Ready 3D printer (Stratasys). Afterward, a magnetoelastic tip was securely twisted into the barrel's tip. Ferrofluid ink (CMS Magnetics) was injected into a replaceable plastic reservoir, and a compressed air cap was applied to ensure the ink remained contained. Next, flexible, thin conductive yarns (Remington Industries 43 HFVP.25) were woven into a coil structure. Finally, the coil was covered with a polyolefin grip (M Wrapping Film, Fisher Scientific).

Characterization of the diagnostic pen

Structural characterization of the magnetoelastic tip and ferrofluid ink was conducted by transmission electron microscopy (Titan Krios High-Res CryoEM), scanning electron microscopy (Zeiss supra 40VP) and micro-computed tomography (CT) (CrumpCAT). The magnetic flux density was quantified using a digital Gauss meter (TM-801, Kanetec). The magnetic hysteresis loop was analyzed using a superconducting quantum interference device (SQUID) magnetometer (MPMS3, Quantum Design). The stress–strain curves were determined by using a dynamic mechanical analyzer (RSA III). The viscosity was evaluated by a rheometer (Anton Paar MCR302 Rheometer). CT image processing was performed by Dragonfly 2022.

Characterization of the electrical performance

The electrical performance measurement system included a function generator (AFG1062, Newark), a power amplifier (PA-151, Labworks), an electrodynamic shaker (ET-126HF, Labworks) and a digital force gauge (Mark-10). Voltage signals were captured using a Stanford low-noise preamplifier (model SR560), while current signals were monitored with a Stanford low-noise current preamplifier (model SR570).

Human studies

All procedures involving healthy participants and patients with PD were conducted in accordance with ethical regulations under the protocol (IRB no. 21-000974) approved by the institutional review board at the University of California, Los Angeles. To recruit patients with PD, study flyers were distributed and physician referrals were requested. All patients were recruited from the Ronald Reagan UCLA Medical Center. The study cohort consisted of 16 individuals, including 3 patients with PD and 13 healthy participants, with an even distribution of sex. Informed consent was obtained from all participants before enrollment. With consent obtained, participants completed designated handwriting tasks using the diagnostic pen. The three selected tasks were based on the protocols from prior clinical research. In addition, having participants draw simple wavy lines, rather than write complex words or sentences, ensured accessibility for nonnative speakers and individuals with reading difficulties. All collected clinical data were securely stored, with access limited to authorized team members only. Participants received gift cards as compensation for their time and contribution. Finally, a convolutional neural network was applied to analyze the handwriting signals for PD diagnostics.

Neural network-assisted personalized handwriting analysis

All collected handwriting signals were standardized by subtracting the mean and dividing by the s.d. The signals were then segmented

into uniform slices. To ensure an unbiased evaluation and prevent test data contamination, data from different individuals were allocated into distinct training and testing sets. Specifically, the data from one patient with PD and three healthy participants were reserved as ‘unseen’ for testing, while the remaining data were used for training and validation. We evaluated three neural-network-based models: a 1D CNN, a 1D CNN with LSTM, and an LSTM, alongside three traditional machine learning methods: random forest, XGBoost and logistic regression. For the traditional machine learning models, we manually extracted nine features from each signal segment: the mean, median, s.d., variance, skewness, kurtosis, minimum, maximum and the sum of fast Fourier transform coefficients. All neural network models were trained for 50 epochs using the Adam optimizer with a learning rate of 0.001 and a batch size of 64. To ensure robustness, each experiment was repeated independently with ten different random seeds. Comprehensive performance metrics, including accuracy, precision, recall and F1 score, were computed and compared across all models.

Statistics and reproducibility

Statistical analyses were conducted using OriginLab. Data are presented as mean \pm s.d., and statistical significance was assessed using a two-tailed *t*-test. The analysis of the pilot human study was performed in a blinded manner. No statistical methods were used to predetermine sample size, and no data were excluded from the analyses.

Reporting summary

Further information on research design is available in the Nature Portfolio Reporting Summary linked to this article.

Data availability

Data supporting the results in this study are available within the Article and its Supplementary Information. Human study data are not publicly available because they contain information that could compromise research participant privacy. Source data are provided with this paper.

Code availability

The machine learning code in this study is available via GitHub at <https://github.com/JCLABShare/PD-PEN>.

References

1. Poebe, W. et al. Parkinson disease. *Nat. Rev. Dis. Primers* **3**, 17013 (2017).
2. Bloem, B. R., Okun, M. S. & Klein, C. Parkinson’s disease. *Lancet* **397**, 2284–2303 (2021).
3. Weintraub, D. et al. The neuropsychiatry of Parkinson’s disease: advances and challenges. *Lancet Neurol.* **21**, 89–102 (2022).
4. Kowal, S. L., Dall, T. M., Chakrabarti, R., Storm, M. V. & Jain, A. The current and projected economic burden of Parkinson’s disease in the United States. *Mov. Disord.* **28**, 311–318 (2013).
5. Armstrong, M. J. & Okun, M. S. Diagnosis and treatment of Parkinson disease: a review. *JAMA* **323**, 548–560 (2020).
6. Dorsey, E. R. et al. Global, regional, and national burden of Parkinson’s disease, 1990–2016: a systematic analysis for the Global Burden of Disease Study 2016. *Lancet Neurol.* **17**, 939–953 (2018).
7. Aarsland, D. et al. Parkinson disease-associated cognitive impairment. *Nat. Rev. Dis. Primers* **7**, 47 (2021).
8. Milekovic, T. et al. A spinal cord neuroprosthesis for locomotor deficits due to Parkinson’s disease. *Nat. Med.* **29**, 2854–2865 (2023).
9. Pavly-Le Traon, A. et al. Clinical rating scales for urinary symptoms in Parkinson disease: critique and recommendations. *Mov. Disord. Clin. Pract.* **5**, 479–491 (2018).

10. Fox, S. H. et al. International Parkinson and movement disorder society evidence-based medicine review: update on treatments for the motor symptoms of Parkinson's disease. *Mov. Disord.* **33**, 1248–1266 (2018).
11. Moustafa, A. A. et al. Motor symptoms in Parkinson's disease: a unified framework. *Neurosci. Biobehav. Rev.* **68**, 727–740 (2016).
12. Tolosa, E., Garrido, A., Scholz, S. W. & Poewe, W. Challenges in the diagnosis of Parkinson's disease. *Lancet Neurol.* **20**, 385–397 (2021).
13. Musubire, A. K. An international exchange observership at Yale University: a Ugandan physician experience. *Neurology* **92**, 582–584 (2019).
14. Höglunger, G. U. et al. A biological classification of Parkinson's disease: the SynNeurGe research diagnostic criteria. *Lancet Neurol.* **23**, 191–204 (2024).
15. Sulzer, D. & Edwards, R. H. The physiological role of α -synuclein and its relationship to Parkinson's disease. *J. Neurochem.* **150**, 475–486 (2019).
16. Pereira, J. B. et al. DOPA decarboxylase is an emerging biomarker for Parkinsonian disorders including preclinical Lewy body disease. *Nat. Aging* **3**, 1201–1209 (2023).
17. Wagner, S. K. et al. Retinal optical coherence tomography features associated with incident and prevalent Parkinson disease. *Neurology* **101**, e1581–e1593 (2023).
18. Lotankar, S., Prabhavalkar, K. S. & Bhatt, L. K. Biomarkers for Parkinson's disease: recent advancement. *Neurosci. Bull.* **33**, 585–597 (2017).
19. Schiess, N. et al. Six action steps to address global disparities in Parkinson disease: a World Health Organization priority. *JAMA Neurol.* **79**, 929–936 (2022).
20. Impedovo, D. & Pirlo, G. Dynamic handwriting analysis for the assessment of neurodegenerative diseases: a pattern recognition perspective. *IEEE Rev. Biomed. Eng.* **12**, 209–220 (2019).
21. Broeder, S. et al. The effects of dual tasking on handwriting in patients with Parkinson's disease. *Neurosci.* **263**, 193–202 (2014).
22. Barrett, M. J., Wylie, S. A., Harrison, M. B. & Wooten, G. F. Handedness and motor symptom asymmetry in Parkinson's disease. *J. Neurol. Neurosurg. Psychiatry* **82**, 1122–1124 (2011).
23. van der Hoorn, A., Burger, H., Leenders, K. L. & de Jong, B. M. Handedness correlates with the dominant Parkinson side: a systematic review and meta-analysis. *Mov. Disord.* **27**, 206–210 (2012).
24. van der Hoorn, A., Bartels, A. L., Leenders, K. L. & de Jong, B. M. Handedness and dominant side of symptoms in Parkinson's disease. *Parkinsonism Relat. Disord.* **17**, 58–60 (2011).
25. Rosenblum, S., Samuel, M., Zlotnik, S., Erikh, I. & Schlesinger, I. Handwriting as an objective tool for Parkinson's disease diagnosis. *J. Neurol.* **260**, 2357–2361 (2013).
26. Thomas, M., Lenka, A. & Kumar Pal, P. Handwriting analysis in Parkinson's disease: current status and future directions. *Mov. Disord. Clin. Pract.* **4**, 806–818 (2017).
27. Masud, M. K. et al. Superparamagnetic nanoarchitectures for disease-specific biomarker detection. *Chem. Soc. Rev.* **48**, 5717–5751 (2019).
28. Lu, W., Shen, Y., Xie, A. & Zhang, W. Green synthesis and characterization of superparamagnetic Fe_3O_4 nanoparticles. *J. Magn. Magn. Mater.* **322**, 1828–1833 (2010).
29. Jeong, U., Teng, X., Wang, Y., Yang, H. & Xia, Y. Superparamagnetic colloids: controlled synthesis and niche applications. *Adv. Mater.* **19**, 33–60 (2007).
30. Cowley, M. D. & Rosensweig, R. E. The interfacial stability of a ferromagnetic fluid. *J. Fluid Mech.* **30**, 671–688 (1967).
31. Neuringer, J. L. & Rosensweig, R. E. Ferrohydrodynamics. *Phys. Fluids* **7**, 1927–1937 (1964).
32. Rosensweig, R. E. *Ferrohydrodynamics* (Cambridge Univ. Press, 1985).
33. Zhou, Y. et al. Giant magnetoelastic effect in soft systems for bioelectronics. *Nat. Mater.* **20**, 1670–1676 (2021).
34. Qian, L. & Li, D. Use of magnetic fluid in accelerometers. *J. Sens.* **2014**, 375623 (2014).
35. Bailey, R. L. Lesser known applications of ferrofluids. *J. Magn. Magn. Mater.* **39**, 178–182 (1983).
36. Kole, M. & Khandekar, S. Engineering applications of ferrofluids: a review. *J. Magn. Magn. Mater.* **537**, 168222 (2021).
37. Impedovo, D., Pirlo, G., Vessio, G. & Angelillo, M. T. A handwriting-based protocol for assessing neurodegenerative dementia. *Cognit. Comput.* **11**, 576–586 (2019).
38. Balestrino, R. & Schapira, A. H. V. Parkinson disease. *Eur. J. Neurol.* **27**, 27–42 (2020).
39. Kamran, I., Naz, S., Razzak, I. & Imran, M. Handwriting dynamics assessment using deep neural network for early identification of Parkinson's disease. *Future Gener. Comput. Syst.* **117**, 234–244 (2021).
40. Fereshtehnejad, S.-M. et al. Evolution of prodromal Parkinson's disease and dementia with Lewy bodies: a prospective study. *Brain* **142**, 2051–2067 (2019).
41. Zerveas, G., Jayaraman, S., Patel, D., Bhamidipaty, A. & Eickhoff, C. A transformer-based framework for multivariate time series representation learning. In Proc. 27th ACM SIGKDD Conference on Knowledge Discovery & Data Mining 2114–2124 (Association for Computing Machinery, 2021).
42. Wen, Q. et al. Transformers in time series: a survey. In Proc. Thirty-Second International Joint Conference on Artificial Intelligence 6778–6786 (Association for Computing Machinery, 2023).
43. Ahmed, S. et al. Transformers in time-series analysis: a tutorial. *Circ. Syst. Signal Process.* **42**, 7433–7466 (2023).
44. *Classify Time Series Using Wavelet Analysis and Deep Learning* (MATLAB, 2024).
45. Szegedy, C. et al. Going deeper with convolutions. In Proc. IEEE Conference on Computer Vision and Pattern Recognition 1–9 (CVPR, 2015).
46. Zhuang, F. et al. A comprehensive survey on transfer learning. *Proc. IEEE* **109**, 43–76 (2021).
47. Eklund, M. et al. Diagnostic value of micrographia in Parkinson's disease: a study with [^{123}I]FP-CIT SPECT. *J. Neural Transm.* **129**, 895–904 (2022).
48. Urso, D., van Wamelen, D. J., Trivedi, D., Ray Chaudhuri, K. & Falup-Pecurariu, C. in *International Review of Movement Disorders*, Vol. 5 (eds Ferro, A. S. & Monje, M. H. G.) 49–70 (Academic Press, 2023).
49. Mirelman, A., Rochester, L., Simuni, T. & Hausdorff, J. M. Digital mobility measures to predict Parkinson's disease. *Lancet Neurol.* **22**, 1098–1100 (2023).
50. He, T., Chen, J., Xu, X. & Wang, W. Exploiting smartphone voice recording as a digital biomarker for Parkinson's disease diagnosis. *IEEE Trans. Instrum. Meas.* **73**, 1–12 (2024).
51. Yang, Y. et al. Artificial intelligence-enabled detection and assessment of Parkinson's disease using nocturnal breathing signals. *Nat. Med.* **28**, 2207–2215 (2022).
52. Liu, Y. et al. Monitoring gait at home with radio waves in Parkinson's disease: a marker of severity, progression, and medication response. *Sci. Transl. Med.* **14**, eadc9669 (2022).
53. Fereshtehnejad, S.-M., Zeighami, Y., Dagher, A. & Postuma, R. B. Clinical criteria for subtyping Parkinson's disease: biomarkers and longitudinal progression. *Brain* **140**, 1959–1976 (2017).
54. Lin, C.-H. et al. Blood NfL. *Neurology* **93**, e1104–e1111 (2019).
55. Mitchell, T. et al. Emerging neuroimaging biomarkers across disease stage in Parkinson disease: a review. *JAMA Neurol.* **78**, 1262–1272 (2021).

56. Ates, H. C. et al. End-to-end design of wearable sensors. *Nat. Rev. Mater.* **7**, 887–907 (2022).
57. Qamar, S. Healthcare data analysis by feature extraction and classification using deep learning with cloud based cyber security. *Comput. Electr. Eng.* **104**, 108406 (2022).
58. Yang, Y. et al. In-sensor dynamic computing for intelligent machine vision. *Nat. Electron.* **7**, 225–233 (2024).
59. Ni, Y. et al. Visualized in-sensor computing. *Nat. Commun.* **15**, 3454 (2024).
60. Chikwetu, L. et al. Does deidentification of data from wearable devices give us a false sense of security? A systematic review. *Lancet Digit. Health* **5**, e239–e247 (2023).

Acknowledgements

J.C. acknowledges the Vernroy Makoto Watanabe Excellence in Research Award at the UCLA Samueli School of Engineering, the Office of Naval Research Young Investigator Award (award ID N00014-24-1-2065), National Institutes of Health Grant (award ID R01 CA287326), National Science Foundation Grant (award number 2425858), the American Heart Association Innovative Project Award (award ID 23IPA1054908), the American Heart Association Transformational Project Award (award ID 23TPA1141360) and the American Heart Association's Second Century Early Faculty Independence Award (award ID 23SCEFIA1157587). S.L. acknowledges the National Institute of Health (NS126918) and the Broad Stem Cell Research Center, the Jonsson Comprehensive Cancer Center and California NanoSystems Institute at UCLA. G.C. acknowledges the Amazon Doctoral Student Fellowship from Amazon AWS and the UCLA Science Hub for Humanity and Artificial Intelligence. G.C. also acknowledges the Predoctoral Fellowship from the American Heart Association and The VIVA Foundation (award ID 24PRE1193744). T.T. and J.C. acknowledge the Caltech/UCLA joint NIH T32 Training Grant (award ID T32EB027629). We also acknowledge the careful editing from the UCLA Writing Center for a one-on-one personalized writing consultation.

Author contributions

J.C. conceived the idea and guided the entire project. J.C., G.C., Y.Z. and X.Z. designed the experiments, analyzed the data, drew the figures and composed the paper. G.C., T.T. and K.A.C. contributed to the human studies. G.C., X.Z., J.C., Z.L., Z.D. and Y.Z. contributed to the device design, fabrication and characterization. Z.D. and Y.Z.

contributed to the theory study. J.Z., W.W. and G.C. contributed to the machine learning study. J.C. and S.L. contributed to the funding acquisition. G.C., K.A.C., T.T., K.S., S.L. and J.C. revised the paper. All authors have read the paper, agreed to its content and approved the final submission.

Competing interests

J.C. and G.C. are inventors on a provisional patent application (UCLA case no. 2025-283) related to the development and application of the diagnostic pen, filed by the University of California, Los Angeles. The other authors declare no competing interests.

Additional information

Extended data is available for this paper at
<https://doi.org/10.1038/s44286-025-00219-5>.

Supplementary information The online version contains supplementary material available at
<https://doi.org/10.1038/s44286-025-00219-5>.

Correspondence and requests for materials should be addressed to Jun Chen.

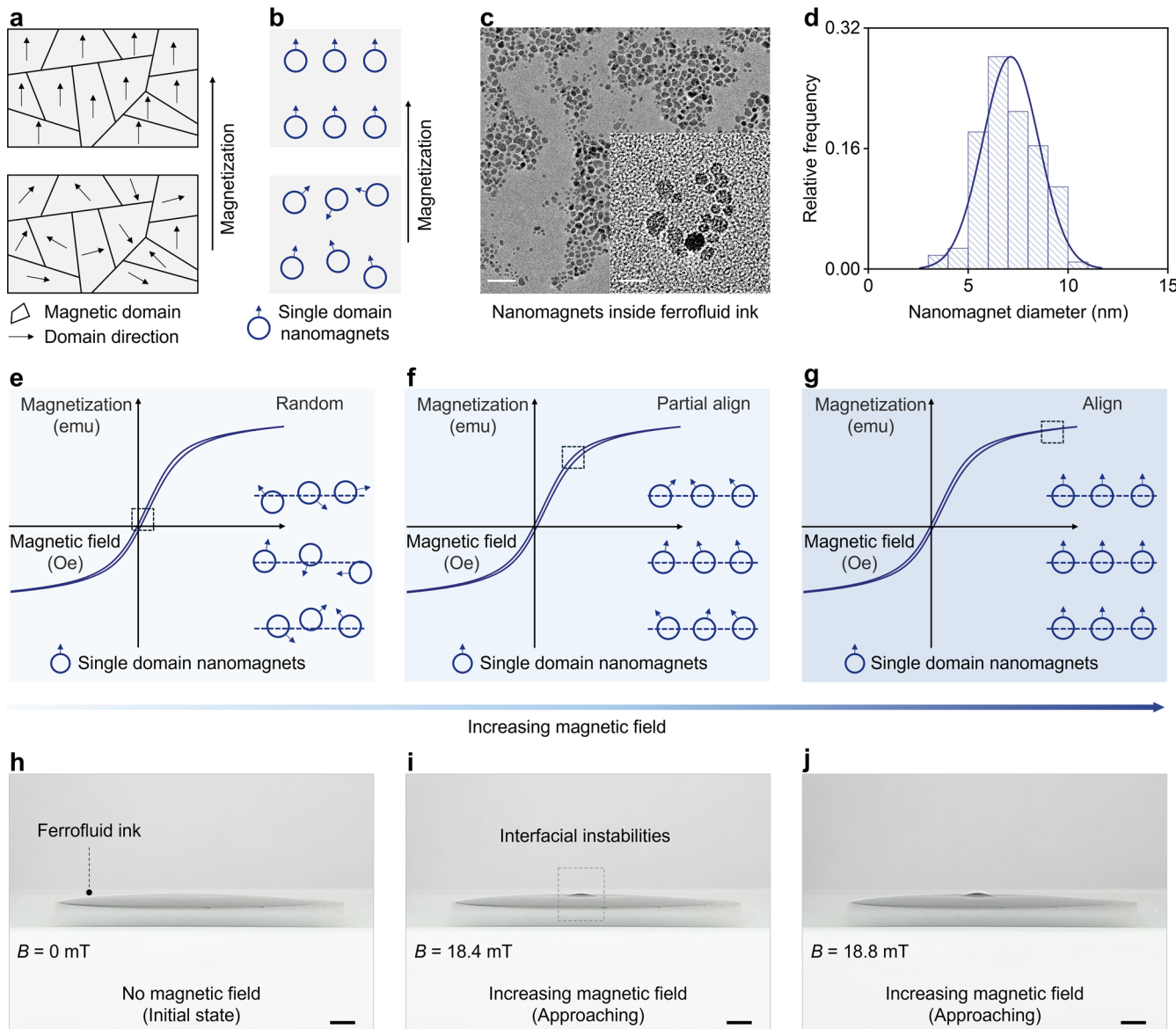
Peer review information *Nature Chemical Engineering* thanks Sibo Cheng, Martin J. McKeown, Huihang Wang and the other, anonymous, reviewer(s) for their contribution to the peer review of this work.

Reprints and permissions information is available at
www.nature.com/reprints.

Publisher's note Springer Nature remains neutral with regard to jurisdictional claims in published maps and institutional affiliations.

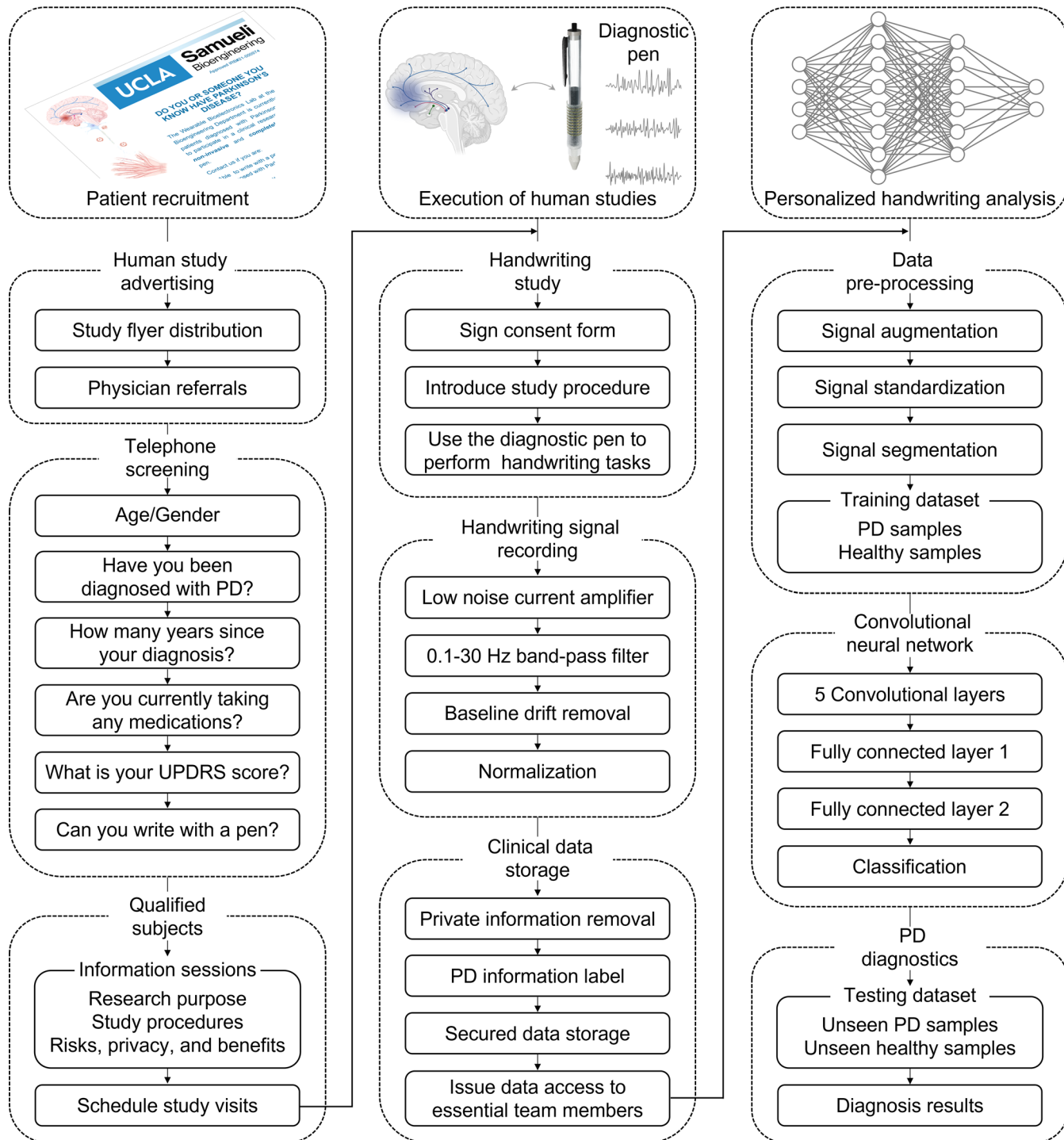
Springer Nature or its licensor (e.g. a society or other partner) holds exclusive rights to this article under a publishing agreement with the author(s) or other rightsholder(s); author self-archiving of the accepted manuscript version of this article is solely governed by the terms of such publishing agreement and applicable law.

© The Author(s), under exclusive licence to Springer Nature America, Inc. 2025



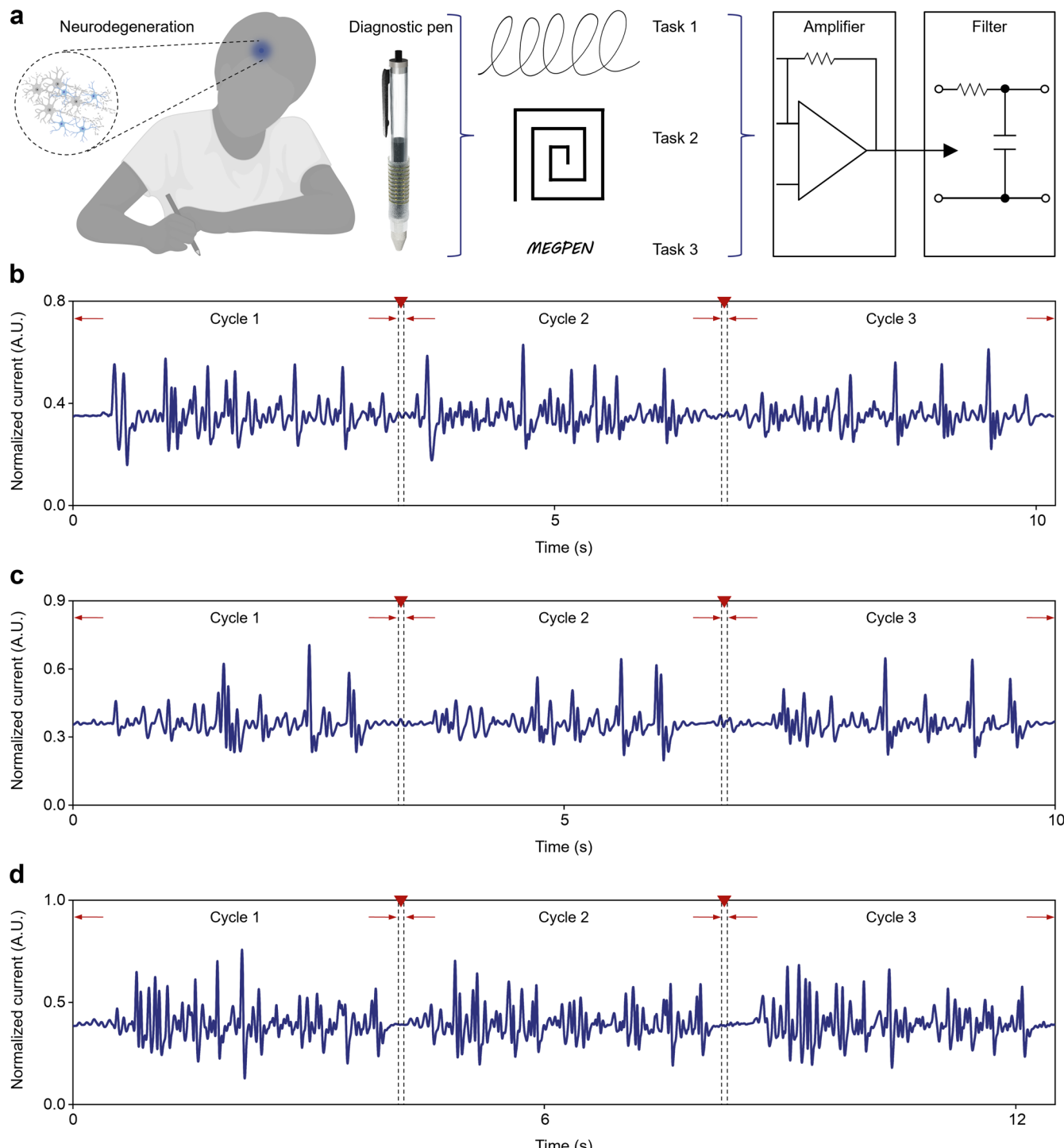
Extended Data Fig. 1 | Magnetic properties and normal field instability of the ferrofluid ink. **a**, The ferromagnetic material is composed of tiny magnetic domains with magnetic spins. **b**, The superparamagnetic ferrofluid ink has a quick response to the external magnetic field and minimal hysteresis. **c**, A transmission electron microscopy image of the single domain nanomagnets inside the ferrofluid ink. Scale bar, 40 nm. Inset is the enlarged view. Scale bar, 10 nm. **d**, These single domain nanomagnets have a particle diameter of $7.13 \pm 1.40 \text{ nm}$. **e-g**, Magnetic hysteresis loops of the ferrofluid ink. **(e)** Under a low external magnetic field, the single domain nanomagnets exhibit a near-random distribution due to minimal magnetic interactions. **(f)** As the external magnetic

field increases, the nanomagnets begin to partially align along the field direction. **(g)** With a further increase in the magnetic field, the single domain nanomagnets become predominantly aligned with the external magnetic field. **h-j**, Surface topography of the ferrofluid ink under increasing external magnetic fields, resulting from the balance between surface tension, gravity, and electromagnetic stress. **(h)** Initial state of the substrate containing the ferrofluid ink. **(i)** A high-speed camera captures the frame where the spike pattern is observed. **(j)** Closer proximity of the external magnetic field leads to larger and more pronounced spike patterns. Scale bars, 1.5 mm.



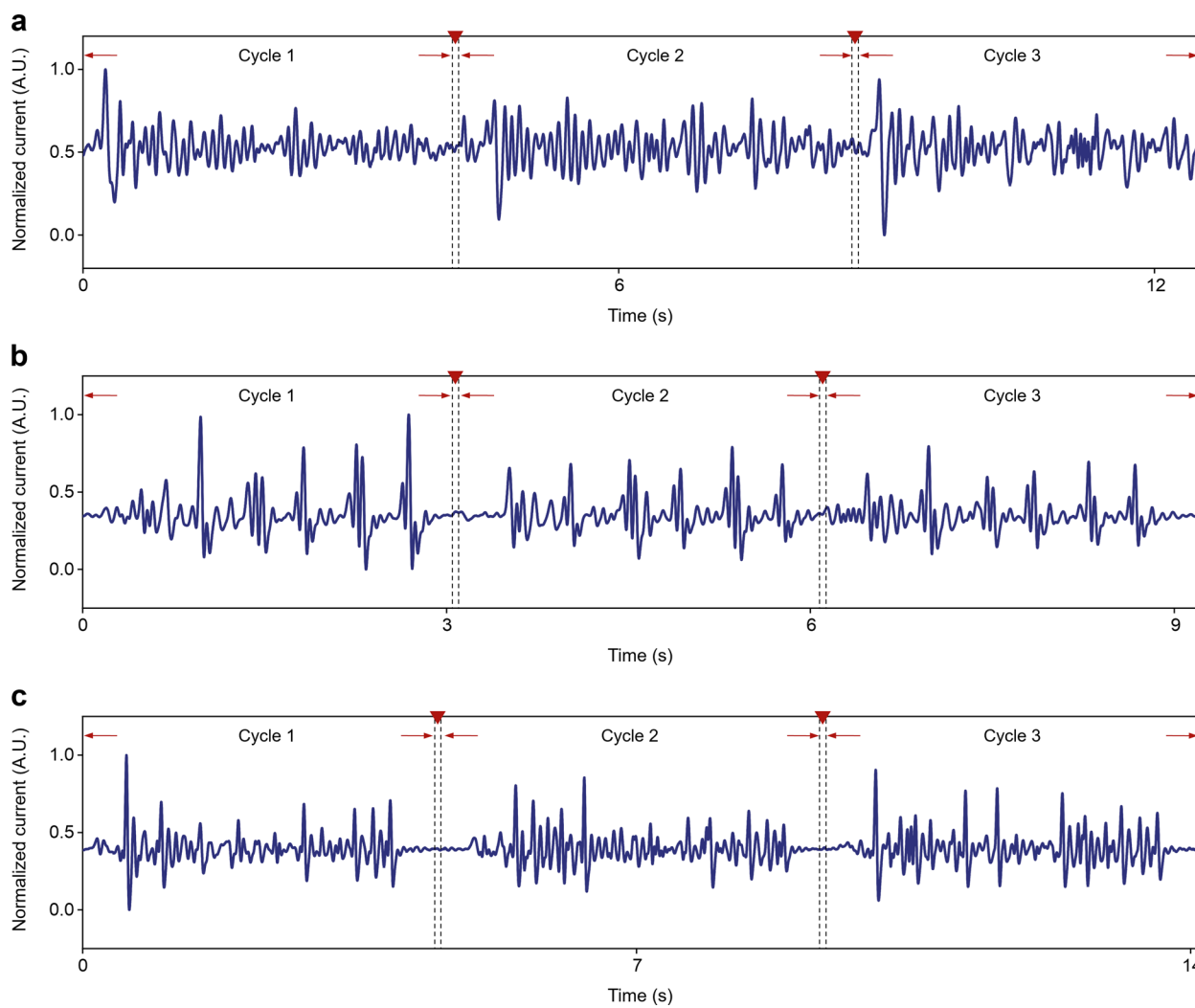
Extended Data Fig. 2 | Block diagram showing the design of the pilot human study. To recruit the participants, study flyers are distributed, and physician referrals are requested. Telephone screenings and information sessions ensure that participants qualify according to specific inclusion and exclusion criteria. With informed consent, participants write specific tasks using a diagnostic pen.

Collected clinical data is securely stored with authorized access restricted to essential team members. Finally, a convolutional neural network analyzes the handwriting signals for PD diagnostics. Figure partially created with [BioRender.com](#).



Extended Data Fig. 3 | Personalized handwriting analysis. **a**, System-level design of using the diagnostic pen for personalized handwriting analysis. **b**, Current signals recorded while using the diagnostic pen to draw continuous wavy lines (Task 1) for three cycles on the surface. **c**, Current signals recorded

while using the diagnostic pen to draw spirals (Task 2) for three cycles on the surface. **d**, Current signals recorded while using the diagnostic pen to write letters (Task 3) for three cycles on the surface. A.U., arbitrary units. Panel **a** partially created with [BioRender.com](#).



Extended Data Fig. 4 | Handwriting signal analysis for in-air handwriting tasks. **a**, Representative current signals from a recruited participant using the diagnostic pen to draw continuous wavy lines (Task 1) for three cycles in the air. **b**, Representative current signals from a recruited participant using the

diagnostic pen to draw spirals (Task 2) for three cycles in the air. **c**, Representative current signals from a recruited participant using the diagnostic pen to write letters (Task 3) for three cycles in the air.

Corresponding author(s): Jun Chen

Last updated by author(s): Apr 3, 2025

Reporting Summary

Nature Portfolio wishes to improve the reproducibility of the work that we publish. This form provides structure for consistency and transparency in reporting. For further information on Nature Portfolio policies, see our [Editorial Policies](#) and the [Editorial Policy Checklist](#).

Statistics

For all statistical analyses, confirm that the following items are present in the figure legend, table legend, main text, or Methods section.

n/a Confirmed

- The exact sample size (n) for each experimental group/condition, given as a discrete number and unit of measurement
- A statement on whether measurements were taken from distinct samples or whether the same sample was measured repeatedly
- The statistical test(s) used AND whether they are one- or two-sided
Only common tests should be described solely by name; describe more complex techniques in the Methods section.
- A description of all covariates tested
- A description of any assumptions or corrections, such as tests of normality and adjustment for multiple comparisons
- A full description of the statistical parameters including central tendency (e.g. means) or other basic estimates (e.g. regression coefficient) AND variation (e.g. standard deviation) or associated estimates of uncertainty (e.g. confidence intervals)
- For null hypothesis testing, the test statistic (e.g. F , t , r) with confidence intervals, effect sizes, degrees of freedom and P value noted
Give P values as exact values whenever suitable.
- For Bayesian analysis, information on the choice of priors and Markov chain Monte Carlo settings
- For hierarchical and complex designs, identification of the appropriate level for tests and full reporting of outcomes
- Estimates of effect sizes (e.g. Cohen's d , Pearson's r), indicating how they were calculated

Our web collection on [statistics for biologists](#) contains articles on many of the points above.

Software and code

Policy information about [availability of computer code](#)

Data collection

Structural analysis was performed utilizing transmission electron microscopy (Titan Krios High-Resolution CryoEM), scanning electron microscopy (Zeiss Supra 40VP), and micro-CT (CrumpCAT). Magnetic flux density measurements were conducted using a digital Gauss meter (TM-801, Kanetec Co., Ltd). Magnetic hysteresis properties were characterized with a SQUID magnetometer (MPMS3, Quantum Design). Stress-strain curves were determined using a dynamic mechanical analyzer (DMA, RSA III). The viscosity was evaluated by a rheometer (Anton Paar MCR302 Rheometer). Voltage signals were captured using a Stanford low-noise preamplifier (model SR560), while current signals were monitored with a Stanford low-noise current preamplifier (model SR570).

Data analysis

For data visualization and analysis, OriginLab 2021 and MATLAB 2024 were employed. Image processing was performed using Dragonfly 2022.

For manuscripts utilizing custom algorithms or software that are central to the research but not yet described in published literature, software must be made available to editors and reviewers. We strongly encourage code deposition in a community repository (e.g. GitHub). See the Nature Portfolio [guidelines for submitting code & software](#) for further information.

Data

Policy information about [availability of data](#)

All manuscripts must include a [data availability statement](#). This statement should provide the following information, where applicable:

- Accession codes, unique identifiers, or web links for publicly available datasets
- A description of any restrictions on data availability
- For clinical datasets or third party data, please ensure that the statement adheres to our [policy](#)

Data availability. Data supporting the results in this study are available within the Article and its Supplementary Information. Source data are provided with this paper. Human study data are not publicly available because they contain information that could compromise research participant privacy.

Code availability. The machine learning code in this study is available via GitHub at <https://github.com/JCLABShare/PD-PEN>.

Human research participants

Policy information about [studies involving human research participants and Sex and Gender in Research](#).

Reporting on sex and gender

[Sex or gender was not a factor in the study design.](#)

Population characteristics

The study cohort consisted of 16 individuals, including 3 PD patients and 13 healthy controls, with an even distribution of sex.

Recruitment

PD patients were recruited through physician referrals from the Ronald Reagan UCLA Medical Center, with specific inclusion and exclusion criteria set to maintain a focused and relevant participant group.

Ethics oversight

All procedures involving healthy subjects and PD patients were conducted in accordance with ethical regulations under the protocol (IRB#21-000974) approved by the Institutional Review Board at the University of California, Los Angeles. To recruit PD patients, study flyers were distributed, and physician referrals were requested. All patients were recruited from the Ronald Reagan UCLA Medical Center. The study cohort consisted of 16 individuals, including 3 PD patients and 13 healthy controls, with an even distribution of sex. Informed consent was obtained from all participants prior to enrollment. With consent obtained, participants completed designated handwriting tasks using the diagnostic pen. All collected clinical data were securely stored, with access limited to authorized team members only. Participants received gift cards as compensation for their time and contribution.

Note that full information on the approval of the study protocol must also be provided in the manuscript.

Field-specific reporting

Please select the one below that is the best fit for your research. If you are not sure, read the appropriate sections before making your selection.

Life sciences

Behavioural & social sciences

Ecological, evolutionary & environmental sciences

For a reference copy of the document with all sections, see nature.com/documents/nr-reporting-summary-flat.pdf

Life sciences study design

All studies must disclose on these points even when the disclosure is negative.

Sample size

The sample sizes for the human study were determined after an in-depth examination of literature standards for proof-of-concept experiments and thorough discussions with physicians, taking into consideration the availability of patient resources.

Data exclusions

No data exclusion.

Replication

All replication attempts were successful when adhering to the device fabrication and sensing testing processes described in the paper. The conclusions were drawn from the analysis of multiple experiments.

Randomization

The fabricated smart pens were randomly allocated to the human subjects in this study, while randomization was not applied in the other studies. As the other studies focus on specifically the mechanical properties, magnetic flux density, and sensing signal generation—under objective and standardized testing conditions. The emphasis was on standard characterization rather than on the variability that randomization is intended to address.

Blinding

The analysis of the human study was conducted in a blinded manner. Blinding was not applicable to other studies because the data were acquired and analyzed using software with objective standards, making blinding irrelevant to the data analysis.

Reporting for specific materials, systems and methods

We require information from authors about some types of materials, experimental systems and methods used in many studies. Here, indicate whether each material, system or method listed is relevant to your study. If you are not sure if a list item applies to your research, read the appropriate section before selecting a response.

Materials & experimental systems

n/a	Involved in the study
<input checked="" type="checkbox"/>	Antibodies
<input checked="" type="checkbox"/>	Eukaryotic cell lines
<input checked="" type="checkbox"/>	Palaeontology and archaeology
<input checked="" type="checkbox"/>	Animals and other organisms
<input checked="" type="checkbox"/>	Clinical data
<input checked="" type="checkbox"/>	Dual use research of concern

Methods

n/a	Involved in the study
<input checked="" type="checkbox"/>	ChIP-seq
<input checked="" type="checkbox"/>	Flow cytometry
<input checked="" type="checkbox"/>	MRI-based neuroimaging